High-optical-quality nanosphere lithographically formed InGaAs quantum dots using molecular beam epitaxy assisted GaAs mass transport and overgrowth

Xifeng Qian,[a] Shivashankar Vangala, Daniel Wasserman, and William D. Goodhue
Department of Physics and Applied Physics, Photonics Center, University of Massachusetts Lowell, Lowell, Massachusetts 01854

Optically active, highly uniform, cylindrical InGaAs quantum dot (QD) arrays have been fabricated using nanosphere lithography combined with Bromine ion-beam-assisted etching and molecular beam epitaxy (MBE)-assisted GaAs mass transport. Previously fabricated QD nanopillar arrays showed significant degradation of optical properties due to the etch damage. Here, a novel mass transport process in a Riber 3200 was performed to encapsulate the lithographically defined InGaAs disk QDs in a GaAs matrix, resulting in the passivation of the etch-damaged QD sidewall layer. Photoluminescence emission intensity following the mass transport process increased by a magnitude of 4–10 as compared to that from unprocessed nanopillar sample. In addition, a PL peak energy redshift was observed after mass transport, presumably due to the decrease in the lateral barrier potential from vacuum to GaAs, as well as the elimination of the depletion layer. Furthermore, the mass transport process in the high vacuum MBE environment enables GaAs overgrowth with few defects and dislocations following mass transport for surface planarization. PL emission intensity increased by an additional factor of 4 following GaAs overgrowth, bringing the QD intensity to $\frac{1}{2}$ of that of the original single quantum well. Thus, the potential of the MBE-assisted mass transport process has been demonstrated to fabricate high optical quality InGaAs quantum dots encapsulated in a GaAs matrix for device applications. © *2010 American Vacuum Society.* [DOI: 10.1116/1.3273941]

I. INTRODUCTION

The incorporation of quantum dot (QD) nanostructures capable of three dimensional (3D) charge carrier confinement into epitaxially grown semiconductor material was first demonstrated in the 1980s, using the Stranski–Krastanow (SK) self-assembled (SA) growth method.[1] The growth of multiple layers of SK QDs occurs with relatively few defects, resulting in QDs with high density and optical quality. Because of this, the SK growth technique has been widely used for the development of QD devices such as low threshold QD lasers,[2] single-photon emitters,[3] and high temperature infrared photodetectors.[4] However, the SK growth process results in QDs with large size fluctuations and inhomogeneous strain distributions, which limit its potential applications. Recently, nanolithography-based approaches to QD fabrication, achieved by nanopatterning epitaxial grown quantum wells[5] (QWs) have demonstrated the requisite dot size, shape, and uniformity for optoelectronic applications. However, traditional nanolithographic techniques, such as electron beam lithography,[6] focused ion beam lithography[7] or nanoimprint lithography[8] can be complex, time consuming, or too expensive to be widely incorporated into the large scale QD-based optoelectronic device research and development. An additional challenge associated with nanolithographically defined, etched QD fabrication is the etch-related sidewall damage to the QD structures resulting from tradi-

tional dry etching techniques,[9] or the surface states produced by wet etching processes,[10] both of which result in the degradation of the nanostructures' optical properties.

The cost of the nanolithography process can be significantly reduced by the utilization of nanosphere lithography (NSL),[11] an inexpensive alternative nanolithographic technique, for the nanopatterning of the QW substrate. NSL is an inherently parallel and high throughput process. It uses a two-dimensional (2D), self-assembled, highly ordered, and close-packed nanosphere array as a template or mask to transfer a nanoscale pattern to the epigrown semiconductor substrate. This technique can be easily adopted in the semiconductor fabrication process, or in smaller scale research laboratories, using a conventional spin-coat setup. Due to its high throughput and low cost, NSL has shown great potential in nanostructure patterning.[12] The diameters of the nanospheres can be selected from 20 nm to 2 μm, resulting in QD density of 3×10^{11} to 3×10^7 cm^{-2}, respectively. In this work 350 nm diameter nanospheres are used, producing an InGaAs QD pillar density of 1×10^9 cm^{-2}.[13] This article explored 300–350 nm diameter nanospheres and at this specific diameter ordered from the vendor the scanning electron microscope (SEM)-measured diameter deviation was about ±3%. The O$_2$ plasma trimming process, described in Ref. 13, increased the diameter deviation to about ±5%. The dry and the wet etch trimming techniques also produce some variations that have not been statistically evaluated but would be similar for all top-down lithographic processes. Recently, we demonstrated the realization of optically active,

---

[a]Electronic mail: xifeng_qian@student.uml.edu

uniform nanopillar arrays of InGaAs QDs in a GaAs matrix.[13] In addition, the etch process used to form the QD pillar arrays often results in the degradation of QD optical properties due to the etch damage to the nanopillar surface and open sidewalls. Such an effect is evident in the significant reduction in photoluminescence emission intensity from these structures as compared to the emission from the original epigrown semiconductor QW. In this work, we demonstrate how the use of a novel high temperature GaAs mass transport (MT) technique can be implemented to provide lateral carrier confinement and recovery of the etch-damaged layer. This process results in a significant improvement in the optical properties of the nanopatterned QDs. A laterally inward etched InGaAs QD nanopillar provides the possibility for GaAs to mass transport from the vertical cladding layers of InGaAs layer of the nanopillar, laterally to the sidewall along the InGaAs layer, providing 3D encapsulation of the InGaAs QD with GaAs. As a result, InGaAs does not interface directly to the vacuum, thus eliminating surface Fermi level pinning effect for InGaAs QD material.[14] Moreover, the high temperature MT process can also repair the surface damage of the previously open sidewalls. Consequently, the nonradiative lifetime is increased and thus electron and hole radiative recombination rate is increased, resulting in improved optical properties of the nanostructures. The MT process under different conditions has been demonstrated for the fabrication of InGaAs QW lasers with buried heterostructure designs[15] and for the surface planarization of GaAs grating grooves.[16]

II. EXPERIMENT

In this experiment, we apply the MT process to nanosphere lithographically defined quantum dot structures, where it acts as a surface passivation and encapsulation technique, with significant potential for the development of high optical quality nanolithographically defined QDs. The MT was investigated using an ultrahigh vacuum (UHV) molecular beam epitaxy (MBE) system. First, The $In_{0.2}Ga_{0.8}As$ QD nanopillars[13] were fabricated by NSL-patterning and subsequent dry etching of a MBE-grown QW structure consisting of a 5 nm thick single InGaAs QW buried under a 50 nm GaAs cap layer. The resulting GaAs/InGaAs/GaAs nanopillars, approximately 150 nm in height, were then selectively etched for 10 s using a wet chemical etchant of citric acid/hydrogen peroxide with volume ration of 2:1.[17] The laterally etching of the nanopillars serves two purposes in the subsequent GaAs MT process, preventing In diffusion and migration at the open sidewalls and allowing the reflowing GaAs to entirely encapsulate the InGaAs quantum dot. Following the selective wet etch of the InGaAs layer, the QD samples were treated at high temperature for mass transport. This process was performed in a Riber 3200 MBE system equipped with an As cracker cell. The sample was mounted on the temperature controlled substrate holder in the MBE system. The As cracker tip was heated up to 1000 °C to provide a flux beam equivalent pressure (BEP) of 7×10^{-6} Torr of As_2 overpressure for compensation of As
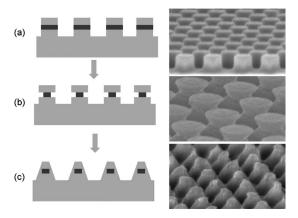

FIG. 1. Schematic illustrations of fabricated QD nanopillar with straight sidewalls (a), laterally inward etched QD pillars after selective etching (b), and laterally confined QDs with GaAs after mass transport process in the UHV, As-rich MBE environment (c), tilt-angled SEM images are shown on the right side.

atom desorption from the sample surface. The samples were then heated to high temperature. A combination of various temperatures (T) and time durations (D) was investigated to obtain optimal conditions for mass transport. A schematic illustration of the lateral etching of the InGaAs QD nanopillars followed by the GaAs MT process as well as corresponding field emission scanning electron microscope (FESEM) images of the results are shown in Fig. 1. The effect of MT process was characterized by FESEM and the corresponding optical properties were measured by low temperature photoluminescence (PL) spectroscopy. Following the MT process, a subsequent 150 nm thick GaAs was overgrown on the samples to ensure a surface planarization for the device fabrication.

III. RESULTS AND DISCUSSIONS

With MBE, we are able to desorb surface oxides before the MT process, and the UHV environment of the MBE prevents any oxide incorporation during the high temperature MT process. This results in clean crystalline surfaces, free of polymer residues and oxides. The MBE MT process on the nanopillar arrays was investigated as a function of temperature and time duration at a fixed As flux stated above. Figure 2 shows SEM images of four mass transported samples from the same QD nanopillar structures. The samples in Figs. 2(a) and 2(b) were processed at 620 °C for 10 and 20 min, respectively, and the samples in Figs. 2(c) and 2(d) were processed at 640 °C for 10 and 20 min, respectively. As shown in the figure, the GaAs on the top of the pillars was transported down the pillars, changing the nanostructures' shape from pillarlike to pyramidal, thereby fully encapsulating the InGaAs QDs in a 3D GaAs matrix. The height of the pyramids in Fig. 2(a) is larger than that in Fig. 2(c), indicating a slower mass transport rate at lower temperature. A similar temperature dependent trend is observed in Figs. 2(b) and 2(d). This can be explained by noting that the atoms on the tops of the nanostructure have more energy at higher temperature, allowing them to break bonds and diffuse to the
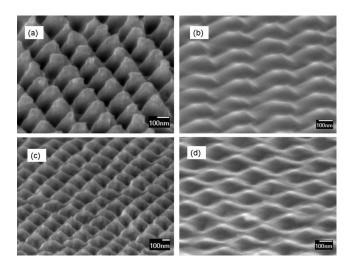
FIG. 2. Tilt-angled SEM images of QD samples processed with MBE mass transport in an As-rich environment at 620 °C for 10 min (a) and 20 min (b) and at 640 °C for 10 min (c) and 20 min.
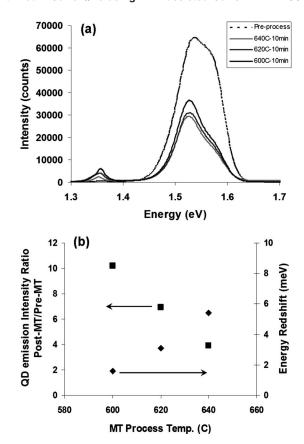

FIG. 3. Low temperature PL spectra of pre- and post-MBE mass transport processed samples (a) (excitation energy density of 100 W/cm²) and QD emission intensity ratio of post-MT/pre-MT and PL peak energy redshift depend on process temperature (b).

adjacent valleys, seeking more stable positions. This process will continue until a surface planarization is reached or the temperature is lowered. When 150 nm high nanopillars are used, pyramids with sidewalls of 60° and heights of 150 nm were formed after MT at 620 °C for 10 min. After mass transport for 20 min on the same sample, the resulting pyramids were only 80 nm in height. Therefore, the mass transport rate at 620 °C can be roughly estimated to be 3.5 nm/s, while for mass transport at 640 °C, this rate is estimated to be 5 nm/s.

The PL results from the MBE mass transported samples showed that no PL emission was observed from the samples in Figs. 2(b) and 2(d). This is a result of excessive mass transport. In the original epitaxially grown SQW structure, the InGaAs layer was only 50 nm below the surface. During the MT process, one can imagine the top monolayer of GaAs diffusing first to the bottom of the pillar, followed by the next monolayer of GaAs, and so on. Once all of the GaAs layers above InGaAs layer have diffused, the InGaAs layer will be exposed to the surface. Because In atoms have much lower desorption temperature than Ga, the In atoms will quickly be desorbed from the sample surface. Even if the In atoms are not fully desorbed under the As overpressure, they may intermix with the surrounding GaAs matrix or diffuse broadly across the sample, resulting in an effective removal of the QW or QD from the mass transported material. In either case, no PL emission from the InGaAs would be measured. However, for those QDs are still remaining after MT, PL emission from InGaAs QDs can be observed. The PL results for pre- and postmass transport processed samples at various temperatures are shown in Fig. 3(a). The preprocessed sample is an InGaAs QD nanopillar with diameter of approximate 200 nm. The other three samples were treated at 600, 620, and 640 °C, respectively for 10 min in the MBE system. Figure 3(a) showed both emissions from QD and bulk GaAs. The intensities of the GaAs band edge PL from the mass transported samples were found to be approxi-

mately half the intensity of that from the preprocessed sample. However, the PL intensities of the QDs increased dramatically for all mass transport recipes shown, with this increase weakened with increasing processing temperature, shown in Fig. 3(b) as black squares. From the 600 °C processed sample, the QD PL intensity increased by a factor of 10, while the 620 and 640 °C processed samples demonstrated PL intensity increases of factors of 6.95 and 3.9, respectively. In addition to the QD PL intensity, an energy redshift of the processed sample was also observed and found to be temperature dependent, also shown in Fig. 3(b) as black diamonds. These energy redshifts compared to QD from unprocessed sample were approximately 1.6 meV from 600 °C processed sample, 3.1 meV from 620 °C processed sample, and 5.4 meV from 640 °C processed sample. These energy redshifts are presumably due to the decrease in the lateral barrier potential from vacuum to GaAs, as well as the elimination of the depletion layer since the InGaAs layer does not interface directly with vacuum. Moreover, the mass transport process resulted in the QD emission linewidth broadening. The PL full width at half maximum (FWHM) from the QDs was measured and found to be 18 meV for the preprocessed sample, 20 meV for the 600 °C processed sample, 30 meV for the 620 °C processed sample, and 25 meV for the 640 °C processed sample. In sum, the PL from the 600 °C, 10 min mass transport processed sample
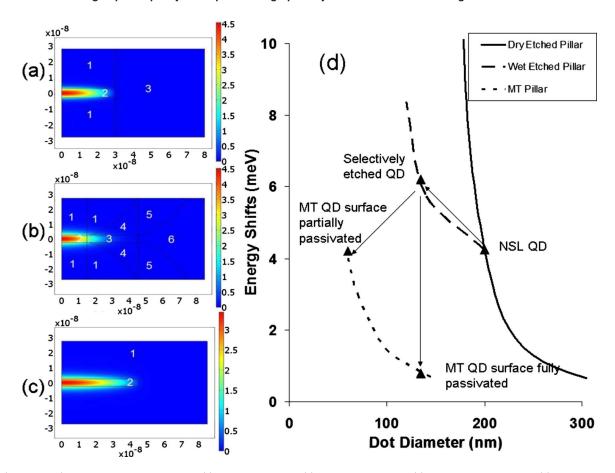
FIG. 4. (Color online) Ground state wavefunction on (a) As-etched QD disk (1) GaAs cladding layer, (2) InGaAs active layer, and (3) outer dead region; (b) wet etched QD (1) GaAs cladding layer, (2) InGaAs active layer, (3) InGaAs depletion layer, (4) GaAs depletion layer, (5) dead layer, and (6) air; (c) MT QD (1) GaAs matrix and (2) InGaAs dot active layer; and (d) simulation results of energy shifts vs dot diameters for dry etched QD pillars (solid line), wet etched QD pillars from 200 nm dry etched pillar (dashed line) and mass transport processed QD nanostructures from 135 nm wet etched pillar (dotted line). The triangles indicate experimental data for 200 nm dry etched pillar (NSL QD), 135 nm wet etched QD (selectively etched QD), 600 °C MT QD (partially passivated), and 640 °C MT QD (fully passivated).

showed the strongest QD emission intensity with the narrowest spectral linewidth. Above this temperature, the PL intensity drops and size and lateral confinement fluctuation-induced spectral linewidth broadening occurs.

To better understand the above results, a single-band model was developed using COMSOL FEMBLAB (Ref. 18) to calculate the interband transition energy between the 1e-1hh levels, as well as to evaluate the dead layer thickness around the perimeter of QD nanopillars.[13] Given the QD nanostructure geometry determined by SEM and appropriate parameters, such as electron or heavy hole effective masses and band offsets, the energy shifts from the processed samples, when compared to the original SQW, can be calculated. Three geometries of QD samples, (1) dry etched QD pillars with straight sidewalls, (2) laterally selective wet etched QD pillars, and (3) mass transport processed laterally confined QD pyramid, are shown in Figs. 4(a)–4(c) with electron ground state wavefunctions. The calculated energy shifts as a function of physical QD diameter are shown in Fig. 4(d). The shift in the QD 1e-1hh transition energy as a function of geometrical pillar diameter is shown as a solid line in Fig. 4(d) for a dry etched QD nanopillars when a 70 nm dead layer was assumed,[13] reducing the QDs' effective size by

140 nm. Wet etching most likely does not produce such a dead layer, but instead removes the dead layer and at the same time produces a depletion layer in the lateral walls of the QD. This depletion layer is typically formed due to the Fermi level pinning by surface states at the semiconductor-air interface of the nanostructure. Therefore, the energy shift increases when reducing the InGaAs layer diameter by wet chemical etching, shown as a dashed line in Fig. 4(d). After the mass transport process, the effective layer thickness was assumed to increase since some of the dead layer is annealed out at the sufficient high temperature. At the same time, due to the replacement of air with GaAs as the confining material in the QD's *xy*-plane, we assume that the depletion region between the InGaAs/GaAs interface is either eliminated of significantly reduced in the case that all sidewall impurities could not be removed by the MBE-MT process. Here, the energy shift of the QD structure as a function of QD diameter is shown as a dotted line in Fig. 4(d). Because of the weaker lateral confinement and reduced potential energy of GaAs, when compared to vacuum, as well as eliminated depletion layer, the energy shift decreases, showing a redshift as compared to that from the wet etched QD sample. In this experiment, dry etched 200 nm diameter QD nanopillars produced
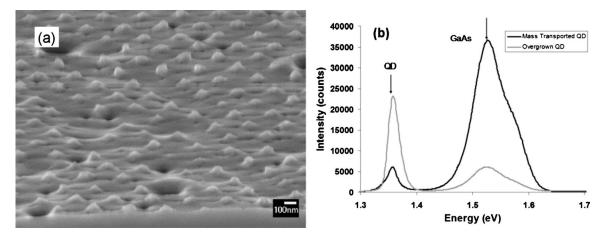
FIG. 5. (a) SEM image of angled view of 150 nm GaAs overgrown sample, and (b) PL spectra of mass transport processed QD samples before overgrowth (black line) and after overgrown with GaAs (gray line) (excitation energy density of 100 W/cm^2). QD intensity increased to approximately $\frac{1}{2}$ of that of the original SQW sample.

PL indicated an active diameter of 60 nm. The theory indicates that this corresponds to a 4.5 meV blueshift. Lateral selective wet etching reduced the geometrical InGaAs layer diameter to 135 nm. PL from this structure indicated a blueshift of 1.7 meV from the As-etched structure. Our interpretation is that the wet etch removed the dead layer leaving a 32 nm thick depletion layer. The model in Fig. 4(b) shows a simulation result. After mass transport, an energy redshift was observed. This energy redshift increases from 1.6 to 5.4 meV with increasing process temperature from 600 to 640 °C. When compared to simulation results shown as a dotted line in Fig. 4(d), this was presumably due to an effective QD lateral size increase with increasing mass transport temperature and the QD dead layer was almost fully passivated when mass transport at 640 °C.

The clean crystalline surface after mass transport in MBE enables the subsequent GaAs overgrowth for a surface planarization with higher quality interfaces. 150 nm GaAs was overgrown on the top of the QD samples, which was first treated at 600 °C for mass transport, and the SEM image was shown in Fig. 5(a). It can be observed that 150 nm GaAs overgrowth is not sufficient to ensure a surface planarization. However, after overgrowth, the optical properties of the material were found to improve significantly, showing an additional increase in PL emission intensity by a factor of 4 in Fig. 5(b). In addition, The FWHM of the overgrown mass transported QDs was only 22 meV, still far less than that from SAQDs,[19] demonstrating a sustainable improved QD uniformity following both the mass transport and overgrowth processes.

IV. CONCLUSIONS

GaAs mass transport process was developed to provide lateral encapsulation of NSL-fabricated InGaAs QDs with GaAs. As a result, the InGaAs QDs do not interface directly with the vacuum and the optical properties of the nanostructures are significantly improved, as demonstrated by the significant increase in PL emission intensities. The PL intensity of the QDs undergoing the mass transport process increased by a factor of 4–10 using the MBE system. The optimal conditions for this process were 600 °C for 10 min with a BEP As flux of 7×10^{-6} Torr in the MBE system. When mass transport took place under these conditions, the PL emission intensity of the sample increased by a factor of 10 as compared to that prior to the process, while the linewidth was nearly unchanged. A PL energy redshift between 1.5 and 5.4 meV was observed from MBE MT processed samples as compared to that from unprocess sample. This is resulted from weaker lateral confinement of GaAs with reduced potential energy and also the elimination of depletion region. Moreover, the mass transport process in the high vacuum MBE environment enables GaAs overgrowth for surface planarization. An additional factor of 4 PL emission intensity increase was observed after GaAs overgrowth. Thus the QD PL intensity after MT and overgrowth was increased to about $\frac{1}{2}$ that of the original SQW sample, with FWHM of 22 meV. This comparison was made by taking the area filling factor into account. Therefore, we have demonstrated the potential of the MBE-assisted mass transport process to fabricate high optical quality InGaAs quantum dots encapsulated in a GaAs matrix for device applications.

[1]L. Goldstein, F. Glas, J. Y. Marzin, M. N. Charasse, and G. Le Roux, Appl. Phys. Lett. **47**, 1099 (1985).
[2]P. M. Varangis, H. Li, G. T. Liu, T. C. Newell, A. Stintz, B. Fuchs, K. J. Malloy, and L. F. Lester, Electron. Lett. **36**, 1544 (2000).
[3]Z. Yuan *et al.*, Science **295**, 102 (2002).
[4]Shiang-Feng Tang, Shih-Yen Lin, and Si-Chen Lee, Appl. Phys. Lett. **78**, 2428 (2001).
[5]P. Ils, M. Michel, A. Forchel, I. Gyuro, M. Klenk, and E. J. Zielinski, J. Vac. Sci. Technol. B **11**, 2584 (1993).
[6]S. G. Rodrigues, M. V. Alves, P. P. González-Borrero, and E. Marega, Jr., Phys. Status Solidi B **232**, 62 (2002).
[7]R. L. Kubena, R. J. Joyce, J. W. Ward, H. L. Garvin, F. P. Stratton, and R. G. Brault, Appl. Phys. Lett. **50**, 1589 (1987).
[8]S. Y. Chou, P. R. Krauss, and P. J. Renstrom, J. Vac. Sci. Technol. B **14**,

4129 (1996).

[9]B. E. Maile, A. Forchel, R. Germann, A. Menschig, H. P. Meier, and D. Grützmacher, J. Vac. Sci. Technol. B **6**, 2308 (1988).

[10]C. Youtsey, G. Bulman, and I. Adesida, J. Electron. Mater. **27**, 282 (1998).

[11]H. W. Deckman and J. H. Dunsmuir, Appl. Phys. Lett. **41**, 377 (1982).

[12]X. Zhang, A. V. Whitney, J. Zhao, E. M. Hicks, and R. P. Van Duyne, J. Nanosci. Nanotechnol. **6**, 1920 (2006).

[13]X. Qian, J. Li, D. Wasserman, and W. D. Goodhue, Appl. Phys. Lett. **93**, 231907 (2008).

[14]H. E. G. Arnot, R. Glew, and S. P. Beaumont, Superlattices Microstruct.

16, 419 (1994).

[15]Z. L. Liau, S. C. Palmateer, S. H. Groves, J. N. Walpole, and L. J. Missaggia, Appl. Phys. Lett. **60**, 6 (1992).

[16]D. Martin, J. Robadey, F. Filipowitz, C. Gourgon, and F. K. Reinhart, J. Cryst. Growth **201–202**, 183 (1999).

[17]G. C. DeSalvo, W. F. Tseng, and J. Comas, J. Electrochem. Soc. **139**, 831 (1992).

[18]R. V. N. Melnik and M. Willatzen, Nanotechnology **15**, 1 (2004).

[19]L. Chu, M. Arzberger, G. Böhm, and G. Abstreiter, J. Appl. Phys. **85**, 2355 (1999).